

# Triplet Contrastive Representation Learning for Unsupervised Vehicle Re-identification

Fei Shen, Xiaoyu Du, Liyan Zhang, Xiangbo Shu, and Jinhui Tang

**Abstract**—Part feature learning is critical for fine-grained semantic understanding in vehicle re-identification. However, existing approaches directly model part features and global features, which can easily lead to serious gradient vanishing issues due to their unequal feature information and unreliable pseudo-labels for unsupervised vehicle re-identification. To address this problem, in this paper, we propose a simple Triplet Contrastive Representation Learning (TCRL) framework which leverages cluster features to bridge the part features and global features for unsupervised vehicle re-identification. Specifically, TCRL devises three memory banks to store the instance/cluster features and proposes a Proxy Contrastive Loss (PCL) to make contrastive learning between adjacent memory banks, thus presenting the associations between the part and global features as a transition of the part-cluster and cluster-global associations. Since the cluster memory bank copes with all the vehicle features, it can summarize them into a discriminative feature representation. To deeply exploit the instance/cluster information, TCRL proposes two additional loss functions. For the instance-level feature, a Hybrid Contrastive Loss (HCL) re-defines the sample correlations by approaching the positive instance features and pushing the all negative instance features away. For the cluster-level feature, a Weighted Regularization Cluster Contrastive Loss (WRCCCL) refines the pseudo labels by penalizing the mislabeled images according to the instance similarity. Extensive experiments show that TCRL outperforms many state-of-the-art unsupervised vehicle re-identification approaches.

**Index Terms**—Vehicle re-identification, contrastive representation learning, loss function.

## I. INTRODUCTION

Vehicle re-identification [1–5] aims to search for the querying vehicle from non-overlapping cameras. It has received wide-spread attention, due to the rapidly growing requirements for traffic video surveillance. The state-of-the-art approaches lie on the supervised learning [6–10] and achieve excellent performance on the public vehicle datasets. However, these approaches require extremely time-consuming and labor-intensive data annotation which limits their use in real scenarios. Therefore, the re-identification community [11–22] now pays wide attention to the unsupervised learning approaches to introduce the unlabeled data.

Contrastive learning is a major technique of unsupervised re-identification. They mostly utilize a memory bank [23–25] to store the recent-step instance/cluster features for the

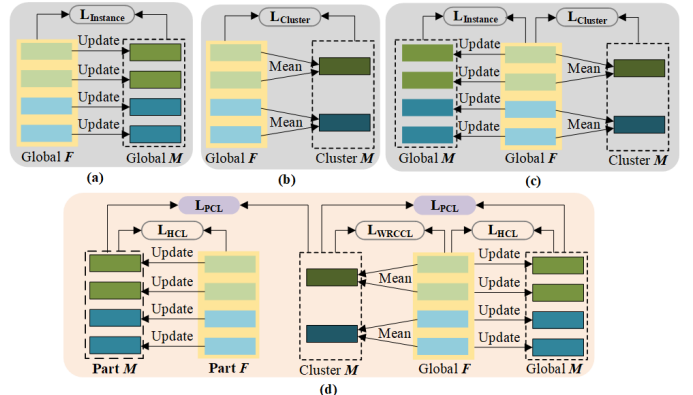


Fig. 1. Comparison of four types of memory-based contrastive learning methods. Here,  $F$  and  $M$  respectively denote features and memory bank. (a) Instance contrastive learning. (b) Cluster contrastive learning. (c) Dual contrastive learning. (d) Our proposed Triplet Contrastive Representation Learning (TCRL) establishes the connection between part features and global features via a proxy of a cluster memory bank. Simultaneously, it computes the loss and updates the features both at instance-level (including part and global) and cluster-level.

next-step contrastive process. The development of contrastive learning is divided into three stages from memory-based structure. Fig. 1 (a) demonstrates the instance-oriented approaches [23, 26–31] that treat each image as a sole class and store all instance features in a global memory bank. Fig. 1 (b) demonstrates the cluster-oriented approaches [32–35] that construct a cluster memory bank with average categorical features. As the former neglects the categorical correlations among the images while the latter neglects the diversity of positive samples (changes caused by perspectives, illuminations, scales, etc.), the dual contrastive [24, 25, 36] approaches shown in Fig. 1 (c) incorporates the global and cluster memory banks to deeply exploit the intra-class information.

Although the contrastive approaches achieve impressive performance, they neglect that the vehicle re-identification task is a fine-grained image retrieval task. Especially vehicles with the same model and color are hardly identified with global features. An intuitive solution is to introduce part and global features like supervised approaches [1, 2, 5, 37–42] at the same time. However, encoder directly models the part features and global features, which is prone to exhibit serious gradient collapse issues because the identity mapping makes them naturally fall into constants (*trivial solutions*), just like [28, 29, 43].

To address the above issues, we propose a Triplet Contrastive Representation Learning (TCRL) framework to establish the connection between part features and global features

Fei Shen, Xiaoyu Du, Xiangbo Shu, and Jinhui Tang are with the School of Computer Science and Engineering, Nanjing University of Science and Technology, Nanjing, 210094, China. e-mail: feishen@njust.edu.cn; duxy@njust.edu.cn; shuxb@njust.edu.cn; jinhuitang@njust.edu.cn.

Liyan Zhang is with the College of Computer Science and Technology, Nanjing University of Aeronautics and Astronautics, Nanjing, 210016, China. e-mail: zhangliyan@nuaa.edu.cn. (Corresponding author: Liyan Zhang.)

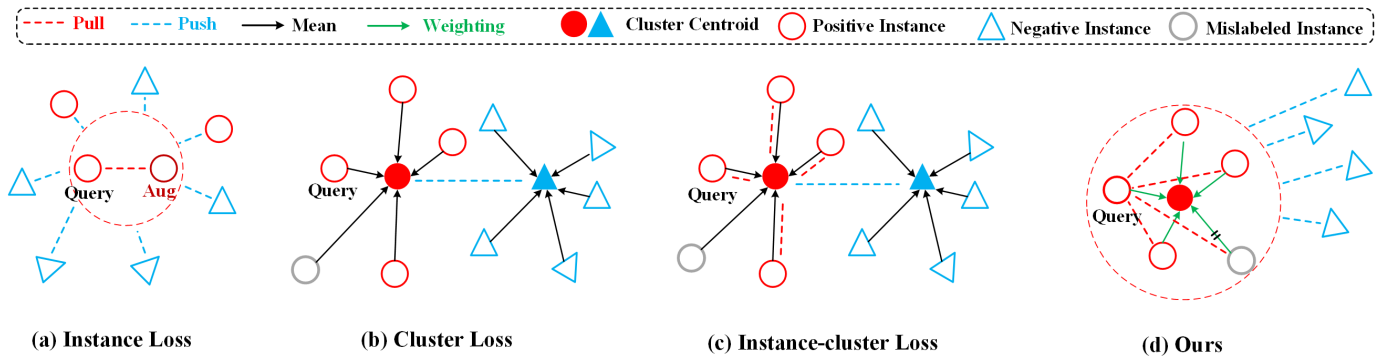


Fig. 2. Illustration for different contrastive learning losses. Different colors and shapes denote different identities. Ours contains proposed Hybrid Contrastive Loss (HCL) and Weighted Regularization Cluster Contrastive Loss (WRCCCL). HCL closes the distance between query samples and instance-level features of positive samples, pushing all negative samples away. WRCCCL refines cluster-level sample correlation and penalizes the mislabeled images by weighting.

naturally via a proxy of a cluster memory bank. As shown in Fig. 1 (d), TCRL devises three memory banks — Part  $M$ , Cluster  $M$ , and Global  $M$  — to store the features of partial images, clustered centroids, and entire images, respectively. To model the part-cluster and cluster-global correlations across the memory banks, TCRL devises a Proxy Contrastive Loss (PCL) that estimates the similarities with Kullback-Leibler Divergence and Euclidean Distance. As the cluster memory bank plays the intermediate role between the part and global memory bank and copes with all the features, it can summarize them into a final discriminative feature representation.

In addition, recent contrastive loss functions may mislead the learned instance correlations. As shown in Fig. 2, we observe that a) the instance loss lacks the correlation between positive instances; b) the cluster loss concentrates on the cluster centroid only; and c) the instance-cluster loss neglects the influence of negative instances. Accordingly, we propose the Hybrid Contrastive Loss (HCL) and Weighted Regularization Cluster Contrastive Loss (WRCCCL). As shown in Fig. 2 (d), HCL adequately exploits the negative information by directly comparing the query instance with all negative instances, and WRCCCL penalizes the mislabeled instances via weighted correlations, respectively.

The main contributions of this paper are summarized as follows:

- A simple Triplet Contrastive Representation Learning framework (TCRL) is proposed to introduce the part features in learning vehicle representations. TCRL bridges the global and part features through three instance/cluster memory banks and proposes a Proxy Contrastive Loss (PCL) to model the adjacent memory banks.
- We devise Hybrid Contrastive Loss (HCL) and Weighted Regularization Cluster Contrastive Loss (WRCCCL) to redefine the instance/cluster correlations. HCL introduces the all individual negative instances into instance-level comparison. WRCCCL weights the correlations to alleviate the impact of mislabeled images.
- We conduct extensive experiments on three large-scale vehicle datasets to demonstrate that the proposed method

is superior to the state-of-the-art unsupervised vehicle re-identification approaches.

## II. RELATED WORK

In this section, we illustrate the related works for vehicle re-identification. We first introduce the contrastive learning approaches in the instance, cluster, and dual learning perspectives. We then present the use of the part features in re-identification approaches.

### A. Instance Contrastive Learning

The instance contrastive learning methods [23, 26–30] regard each image as an individual class and consider two augmented views of the same image as positive pairs and treat others in the same batch as negative pairs. For example, momentum contrast (MoCo) [26] transforms into a dictionary lookup task, using a contrastive loss to learn instance discriminative representations, treating each unlabeled example as a distinct class. Simple framework for contrastive learning of visual representations (SimCLR) [23] regards samples in the current batch as the negative samples. Similarly, Bottom [30] treats each individual sample as a cluster and then progressively groups similar samples into a cluster, generating pseudo labels. Though instance-level contrastive loss performs well in downstream tasks, it performs poorly on re-identification tasks that require correct measurement of inter-class differences on unsupervised target domains.

### B. Cluster Contrastive Learning

The cluster contrastive learning methods [32–35] are initialized with a cluster-level memory dictionary. The clustering algorithms are used to generate corresponding pseudo labels in the above methods. For example, cluster contrast learning (CCL) [34] employs a unique cluster representation to describe each cluster, computing contrast loss at the cluster level. Self-paced contrastive learning (SPCL) [32] proposes a novel self-paced contrastive learning framework that gradually creates a more reliable cluster to refine the memory dictionary features. Uncertainty-aware clustering framework (UCF) [35]

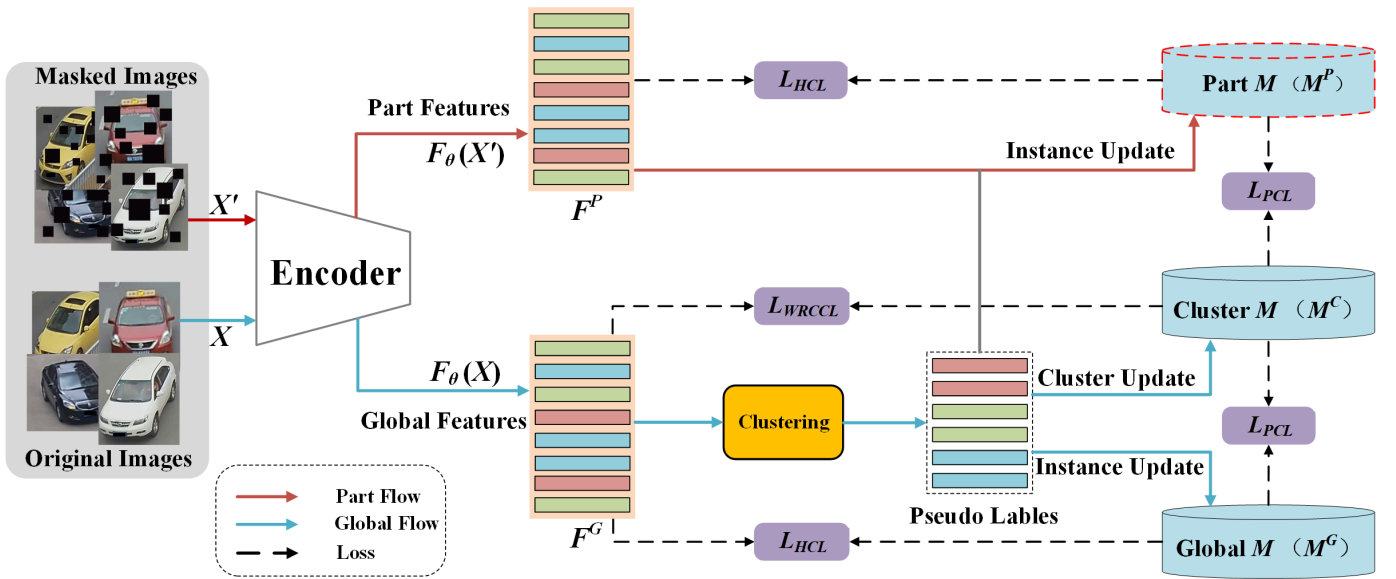


Fig. 3. The framework of the proposed Triplet Contrastive Representation Learning (TCRL), including part memory bank  $M^P$ , cluster memory bank  $M^C$ , and global memory bank  $M^G$ . Here,  $U^P$  and  $U^G$  respectively part and global features. **Training:** Original images are first sampled in mini-batches to generate the corresponding masked images. Then, these two batches of images are fed to the encoder simultaneously to obtain global features and part features. Second, a clustering algorithm is applied to cluster similar global features and assign pseudo labels to them. Third, the part feature of all samples, the average global feature of each cluster, and the global feature of all samples are stored in  $M^P$ ,  $M^C$ , and  $M^G$ , respectively. Finally, the features of three memory banks are updated with momentum via our proposed three loss functions in TCRL. **Inference:** Masked images and part features are only used for training and will be removed for a fair comparison. Thus, we extract features of test images through the encoder, and the cosine distance is applied as the similarity measurement.

proposes a novel hierarchical clustering scheme to promote clustering quality and introduce an uncertainty-aware collaborative instance selection method.

### C. Dual Contrastive Learning

Dual contrastive learning methods [24, 25, 44, 45] are typically initialized with a cluster-level memory dictionary and instance-level memory to distill the advantages from the two parts. Cluster-guided asymmetric contrastive learning (CACL) [25] designs an asymmetric contrastive learning framework to guide the siamese network effectively mine the invariance in feature representation. Hard-sample guided hybrid contrast learning (HHCL) [24] combines cluster centroid contrastive loss with hard instance contrastive loss for unsupervised person re-identification. Besides, there are some others methods. For example, the dual-branch adversarial network (DAN) [44] develops an image-to-image translation network without any annotation for unsupervised vehicle re-identification. Viewpoint-aware progressive clustering (VAPC) [45] divides the entire feature space into different subspaces and then performs a progressive clustering to mine the authentic relationship among samples. However, the unsupervised vehicle re-identification approaches insufficiently model the part features thus impacting the final performance of unsupervised methods.

### D. Part Feature Learning

Part feature learning methods usually divide feature maps into several parts and then individually pool each region, as done in [46–51]. For example, stripe-based and attribute-aware network (SAN) [48] extracts the part features from the visual

appearance of vehicles through a stripe-based branch and an attribute-aware branch. Hybrid pyramidal graph network (HPGN) [47] explores the spatial significance of part features at multiple scales via spatial graph networks (SGNs). Besides, there is also a method of using a typical detector to refine part features in [38, 52–54]. For example, part regularization [52] uses you only look once (YOLO) [55] as a detector to detect parts and feature extraction from part regions. Adaptive attention vehicle re-identification (AAVER) [38] uses a key-point detection module to localizing the part features and use an adaptive key-point selection module to learning the relationship of parts. Although part features have been widely used in supervised re-identification, unsupervised tasks have been challenging due to serious gradient collapse problems.

## III. PROPOSED METHOD

As shown in Fig. 3, the proposed Triplet Contrastive Representation Learning (TCRL) framework consists of three components: (1) a feature encoder module for extracting global and part features, (2) a clustering module for generating pseudo labels, and (3) three memory banks for storing updated features of the dataset, namely part memory bank, cluster memory bank, and instance memory bank. Unlike other unsupervised re-identification methods, the input to feature encode module is two batches of images, i.e., the original and mask images. Specifically, first, we sample a batch of original images and generate corresponding masked images. And we use ResNet50 [56] without a fully connected layer as the feature encode module. Second, these two batches of images are fed to ResNet50 simultaneously to obtain global features and part features. Third, a clustering algorithm (i.e.,

DBSCAN [57]) is applied to cluster similar global features and assign pseudo labels to them. The part feature of all samples, the average global feature of each cluster, and the global feature of all samples are stored in the part memory bank, cluster memory bank, and instance memory bank, respectively. Finally, features of the three memory banks are updated with momentum via TCRL framework. Moreover, TCRL designs three different loss functions, i.e., Proxy Contrastive Loss (PCL), Hybrid Contrastive Loss (HCL), and Weighted Regularization Cluster Contrastive Loss (WRCCCL). More detail about TCRL framework is described as follows.

### A. Preliminaries

Assume that an unlabeled dataset  $X = \{x_1, x_2, \dots, x_n, \dots, x_N\}$  consisting of  $N$  original images. For an original input image  $x_n \in X$ , correspondingly we generate a masked image  $x'_n$ . Similarly, we can get the unlabeled masked dataset  $X' = \{x'_1, x'_2, \dots, x'_n, \dots, x'_N\}$  of  $N$  masked images. We use both  $x_n \in X$  and  $x'_n \in X'$  as input images. The global features  $F^G = \{f_1^G, f_2^G, \dots, f_n^G, \dots, f_N^G\}$  and part features  $F^P = \{f_1^P, f_2^P, \dots, f_n^P, \dots, f_N^P\}$  are obtained from the feature encode module. To guide the contrastive learning, pseudo labels  $Y_K$  are generated by global features through a clustering module. According to the pseudo labels, part memory bank  $M^P$  and global memory bank  $M^G$  are set as the current part features  $F^P$  and global features  $F^G$  before each forward propagation.

Different from the part memory bank  $M^P$  and global memory bank  $M^G$ , the mean global feature vectors of each pseudo labels are initialized with the cluster memory bank  $M^C = \{c_1, c_2, \dots, c_k, \dots, c_K\}$  by

$$c_k = \frac{1}{|M_k^C|} \sum_{f_i^G \in M_k^C} f_i^G, \quad (1)$$

where  $M_k^C$  represent the  $k$ -th cluster set of  $M^C$  that contains all the feature vectors within cluster  $k$  and  $|\cdot|$  denotes the number of features in the set. Noted that the clustering algorithm runs in each epoch, so the number of pseudo labels  $K$  can be updated during the training phase.

### B. Proxy Contrastive Loss

A novel Proxy Contrastive Loss (PCL) is proposed to indirectly model and transform instance-level (i.e., part and global) features via a cluster memory bank. Note that this is not as easy as simply defining a loss function that includes both part and global branch. The reason is that they have different inputs and focus on different areas. This choice is natural that PCL should contain two parts. They make contrastive learning between adjacent memory banks, thus presenting the associations between the part and global features as a transition of the part-cluster and cluster-global associations. Thus, the total of  $L_{PCL}$  consists of two parts as follows,

$$L_{PCL} = \frac{L_{PCL}^G + L_{PCL}^P}{2}, \quad (2)$$

where the  $L_{PCL}^G$  and  $L_{PCL}^P$  denote the proxy contrastive learning loss of global and part features, respectively.

For simplicity we directly use  $q_i$  and  $q'_i$  to represent the features of original-query image and masked-query image through the encoder module, except when specified. Specifically, given the features of original-query image  $q_i$  and the corresponding cluster feature  $c_k$  from cluster memory bank  $M^C$ , we can defined the  $L_{PCL}^G$  as follows,

$$L_{PCL}^G = L_{kl}(z(c_k), z(q_i)) + L_{dl}(q_i, c_k), \quad (3)$$

where  $L_{kl}$  is the kullback-leibler [58] divergence loss, which enables the output logit value of query image  $q_i$  to supervise the output logit value of cluster feature  $c_k$ ;  $z(\cdot)$  denotes the softmax function.  $L_{dl}$  is the euclidean distance loss function to distill the relation between  $q_i$  and  $c_k$  by minimizing the distance.  $L_{dl}$  is formulated as follows:

$$L_{dl}(q_i, c_k) = \|q_i - c_k\|_2, \quad (4)$$

where  $\|\cdot\|_2$  is  $l_2$  normalization function. Correspondingly, based on Eq. (3) and Eq. (4), assuming that features of masked-query image  $q'_i$ , we can calculate  $L_{PCL}^P$  of part feature as follows,

$$L_{PCL}^P = L_{kl}(z(c_k), z(q'_i)) + L_{dl}(q'_i, c_k). \quad (5)$$

Since the cluster memory bank  $M^C$  deals with all the features of vehicle, it can summarize them into a discriminative feature representation.

### C. Hybrid Contrastive Loss

Given the feature of masked-query image  $q'_i$  along with pseudo label  $y_k \in Y_K$ , Hybrid Contrastive Loss (HCL) of the part feature  $L_{HCL}^P$  is formulated as follows,

$$L_{HCL}^P = -\log \frac{\sum_{j \in y_k} \exp \langle q'_i \cdot M_j^P / \tau \rangle}{\sum_{j \in y_k} \exp \langle q'_i \cdot M_j^P / \tau \rangle + \sum_{n \notin y_k} \exp \langle q'_i \cdot M_n^P / \tau \rangle}, \quad (6)$$

where  $M_j^P$  denotes the part features of positive instance with the same pseudo label as  $q'_i$ . Instead,  $M_n^P$  represents the part features of all negative samples from  $M^P$ , i.e., they do not belong to the same pseudo label  $y_k$  as the current query sample  $q'_i$ . The  $\tau$  is a temperature hyper-parameter, and set to 0.05.

In the same way, given the feature of original-query image  $q_i$  along with pseudo label  $y_k \in Y_K$ , the HCL of global feature  $L_{HCL}^G$  is defined as follows,

$$L_{HCL}^G = -\log \frac{\sum_{j \in y_k} \exp \langle q_i \cdot M_j^G / \tau \rangle}{\sum_{j \in y_k} \exp \langle q_i \cdot M_j^G / \tau \rangle + \sum_{n \notin y_k} \exp \langle q_i \cdot M_n^G / \tau \rangle}, \quad (7)$$

According to Eq. (6) and Eq. (7), we calculate the distance between the query image and the feature vector of the instance. Ideally, HCL should be able to pull similar samples together rather than to use the cluster-level features (mean vectors of positive instance) in inter-class instances, like CCL [34]. The reason is that it is necessary to care for richer and differentiated positive sample information. Meanwhile, to add more negative sample information, we treat all samples except positive

samples as negative samples instead of just using the mean vector of negative samples' clusters, such as SPCL [32]. So our proposed HCL can close the distance between query samples and instance-level features of positive samples, pushing all negative samples away.

The two memory banks  $M^P$  and  $M^G$  are updated by using Eq. (8), as follows,

$$\begin{aligned} f_i^P &\leftarrow \alpha f_i^P + (1 - \alpha) q_i' \\ f_i^G &\leftarrow \beta f_i^G + (1 - \beta) q_i, \end{aligned} \quad (8)$$

where  $\alpha, \beta \in [0, 1]$  is a momentum constant used to control the update rate of memory banks.  $\alpha = \beta$  is set as 0.1.

### D. Weighted Regularization Cluster Contrastive Loss

For pseudo labels  $Y_K$ , the results of clustering algorithms may be unreliable and bring noise samples. We observe that images with correct labels are usually dominant, while images with wrong labels are from non-dominant uncertain classes. Therefore, we can judge whether the image belongs to a possible wrong label via measuring the similarity between the current query image and other images with the same pseudo label.

Formally, given the feature of query image  $q_i$  along with pseudo label  $y_k \in Y_K$ , the weight  $w_i$  is designed by using Eq. (9), as follows,

$$w_i = \frac{1}{N} \sum_{j=1}^N \frac{q_i \cdot q_j}{\|q_i\|_2 \|q_j\|_2}, \quad (9)$$

where  $N$  and  $\|\cdot\|_2$  are denote the number with the same pseudo label  $y_k$  as query image  $q_i$  and the  $\ell_2$  normalization function, respectively. Weighted Regularization Cluster Contrastive Loss (WRCCCL)  $L_{WRCCCL}$  is further defined as:

$$L_{WRCCCL} = -w_i \log \frac{\exp \langle q_i \cdot c_k / \tau \rangle}{\sum_{j=1}^K \exp \langle q_i \cdot c_j / \tau \rangle}, \quad (10)$$

where  $c_k$  represent the feature vector with the same pseudo label  $y_k$  as the query image  $q_i$  from cluster memory bank  $M^C$ . According to Eq. (10), we assign a lower weight to the training loss of the uncertain images in intra-class instances, so that the potentially correct images contribute more to cluster contrastive learning. The cluster memory bank  $M^C$  is updated according to Eq. (11), as follows,

$$c_k \leftarrow \gamma c_k + (1 - \gamma) q_i, \quad (11)$$

where  $\gamma \in [0, 1]$  is a momentum constant same as  $\alpha$  and  $\beta$  in Eq. (8). Consistent with the update progress of memory banks  $M^P$  and  $M^G$ , we set  $\gamma = 0.1$  in the following experiments.

Thus, we propose a simple and unified TCRL framework that combining PCL, WRCCCL, and HCL losses. The total loss function  $L_{Total}$  of our proposed TCRL is as follows,

$$L_{Total} = \lambda(L_{PCL}^P + L_{PCL}^G) + \eta(L_{HCL}^P + L_{HCL}^G) + L_{WRCCCL}, \quad (12)$$

where  $\lambda$  and  $\eta$  are hype-parameters, used to control the balance between different losses. Their default value are respectively set to 0.5 and 1.0 via cross-validation.

TABLE I  
THE PERFORMANCE (%) COMPARISON ON VERI776. 'SOURCE' DENOTES THE SOURCE DATASET. BEST AND SECOND-BEST PERFORMANCE ARE IN RED AND BLUE COLOR, RESPECTIVELY.

	Methods	Source	mAP	Rank1	Rank5
<b>Instance</b>	MoCo [26]	None	9.53	24.92	40.61
	SimCLR [23]	None	9.74	25.42	42.94
	SwAV [27]	None	9.78	25.86	42.77
	BYOL [28]	None	9.92	26.38	44.68
	Simsiam [29]	None	10.35	28.84	45.16
	Bottom [30]	None	23.5	63.7	73.4
<b>Cluster</b>	SPCL [32]	VehicleID	38.9	80.4	86.8
	CA-UReID [33]	None	40.08	84.17	88.25
	CCL [34]	None	40.3	84.6	89.2
	UCF [35]	VehicleID	40.5	85.2	88.7
<b>Dual</b>	MGCE-HCL [36]	None	39.28	81.56	87.73
	HHCL [24]	None	40.44	85.33	88.29
	CACL [25]	None	40.92	84.46	88.21
<b>Others</b>	OIM [59]	None	12.2	45.1	62.2
	PUL [60]	None	17.06	55.24	66.27
	HHL [61]	None	17.52	56.2	67.61
	ECN [62]	VehicleID	20.06	57.41	70.53
	DAN [44]	VehicleID	24.85	58.46	70.86
	UDAR [63]	VehicleID	35.8	76.9	85.8
<b>Proposed</b>	ML [64]	VehicleID	36.9	77.8	85.5
	TCRL	None	42.68	87.26	90.75

## IV. EXPERIMENTS AND ANALYSIS

### A. Datasets

1) *VeRi776*: [65] is constructed by 20 cameras in unconstrained traffic scenarios and each vehicle is captured by 2-18 cameras. Following the evaluation protocol of [65], VeRi776 is divided into a training subset containing 37,746 images of 576 subjects and a testing subset including a probe subset of 1,678 images of 200 subjects and a gallery subset of 11,579 images of the same 200 subjects.

2) *VehicleID*: [66] totally includes 221,763 images of 26,267 subjects. The training subset consists of 110,178 images of 13,164 subjects. There are three testing subsets, i.e., Test800, Test1600, and Test2400, for evaluating the performance at different data scales. Specifically, Test800 includes 800 gallery images and 6,532 probe images of 800 subjects. Test1600 contains 1,600 gallery images and 11,395 probe images of 1,600 subjects. Test2400 is composed of 2,400 gallery images and 17,638 probe images of 2,400 subjects. Following the evaluation protocol of [66], for three testing subsets, the division of probe and gallery subsets is implemented as follows: randomly selecting one image of a subject to form the probe subset, and all remaining images of this subject are used to construct the gallery subset. This division is repeated and evaluated 10 times, and the average result is reported as the final performance.

3) *VERI-Wild*: [68] has in total 416,314 images of 40,671 subjects divided into a training subset of 277,797 images of 30,671, and a testing subset of 128,517 images of 10,000 subjects. Different to the VeRi776 [65] and VehicleID [66] captured at day, VERI-Wild also contains images captured at night. Similar to VehicleID [66], the testing subset of VERI-Wild is organized into three different scale subsets, i.e., Test3000, Test5000, and Test10000. Test3000 is composed of 41,816 gallery images and 3000 probe images of 3,000

TABLE II

THE PERFORMANCE (%) COMPARISON ON VEHICLEID AND VEHICLE WILD. BEST AND SECOND-BEST PERFORMANCE ARE IN RED AND BLUE COLOR, RESPECTIVELY. BLANKED ENTRIES LINK TO RESULTS NOT REPORTED IN PREVIOUS WORKS.

Methods	Source	VehicleID						VERI-Wild							
		Test800		Test1600		Test2400		Test3000		Test5000		Test10000			
		mAP	Rank1	mAP	Rank1	mAP	Rank1	mAP	Rank1	mAP	Rank1	mAP	Rank1		
<b>Instance</b>	MoCo [26]	None	27.74	22.68	24.85	19.51	21.83	15.80	None	15.25	38.70	12.06	34.81	9.27	31.22
	Simsiam [29]	None	28.48	23.21	25.17	19.94	22.39	16.55	None	15.66	39.25	12.43	35.39	9.65	31.80
<b>Cluster</b>	SPCL [32]	None	61.74	55.46	58.66	51.58	55.49	47.92	None	34.29	71.38	30.33	64.82	22.67	61.13
	CA-UReID [33]	None	62.88	56.50	59.78	52.32	56.77	49.05	None	36.18	72.53	31.44	65.83	23.92	62.15
	CCL [34]	None	62.97	56.71	60.10	52.55	57.08	49.33	None	<b>36.36</b>	72.41	31.42	65.75	23.86	62.50
<b>Dual</b>	MGCE-HCL [36]	None	62.92	56.69	59.82	52.78	56.82	49.08	None	35.77	72.26	31.15	65.49	23.57	61.84
	HHCL [24]	None	63.60	57.47	60.95	<b>53.48</b>	57.04	50.61	None	36.11	72.60	31.52	65.76	23.86	62.44
	CACL [25]	None	<b>63.83</b>	<b>57.77</b>	<b>61.19</b>	53.25	<b>57.47</b>	<b>50.80</b>	None	36.28	<b>72.94</b>	<b>31.87</b>	<b>66.02</b>	<b>24.33</b>	<b>62.99</b>
<b>Others</b>	PUL [60]	None	43.90	40.03	37.68	33.83	34.71	30.90	None	18.7	52.1	14.9	48.3	10.6	38.2
	DAN [44]	VeRi776	49.53	44.44	43.90	38.97	40.07	35.10	-	-	-	-	-	-	-
	ATTNet [67]	VeRi776	54.01	49.48	49.72	45.18	45.18	40.71	-	-	-	-	-	-	-
	UDAR [63]	VeRi776	59.6	54.0	55.3	48.1	52.9	45.2	None	30.0	68.4	26.2	62.5	20.8	53.7
	ML [64]	VeRi776	61.6	54.8	58.4	51.3	55.0	47.5	-	-	-	-	-	-	-
	VAPC [45]	-	-	-	-	-	-	-	None	33.0	72.1	28.1	64.3	22.6	55.9
	TCRL	None	<b>66.29</b>	<b>60.36</b>	<b>63.74</b>	<b>56.22</b>	<b>61.08</b>	<b>52.93</b>	None	<b>39.08</b>	<b>75.22</b>	<b>34.67</b>	<b>68.59</b>	<b>26.60</b>	<b>64.31</b>

subjects. Test5000 is made up of 69,389 gallery images and 5,000 probe images of 5,000 subjects. Test10000 is consisted of 138,517 gallery images and 10,000 probe images of 10,000 subjects.

B. Implementation Details

Training configurations are summarized as follows. (1) All the experiments are performed with 8 Nvidia Tesla V100 GPUs using the PyTorch [69] toolbox with FP16 training. (2) We adopt ResNet50 [56] as the backbone of the feature encoder and initialize the model with the parameters pre-trained on ImageNet. (3) The input image is resized 224 × 224. Random horizontal flip and random crop are used for the data augmentation. Both probabilities of horizontal flip and crop are set to 0.5, respectively. Noted that the occlusion area of the mask image generated by the original image is 0.2-0.4 times that of the original image, and the aspect ratio is 1. (4) Each mini-batch includes 192 vehicle images, which includes 48 subjects and each subject holds 4 images. For the training phase, we use DBSCAN [57] for clustering to generate pseudo labels. (5) The Adam optimizer is applied to train parameters with weight decays 5 × 10<sup>-4</sup>. There are 50 epochs for the training process. The learning rates are initialized to 3 × 10<sup>-4</sup>, and they are linearly warmed up to 3 × 10<sup>-2</sup> in the first 10 epochs. After warming up, the learning rates are maintained at 3 × 10<sup>-2</sup> from 11-th to 30-th epochs. Then, the learning rates are reduced to 3 × 10<sup>-3</sup> between 31-th and 50-th epochs. Moreover, during the testing phase, the cosine distance of the global average pooling layer is applied as the similarity measurement for unsupervised vehicle re-identification.

C. Performance Comparison

For a clear presentation, we roughly divide the existing methods into four categories, namely “Instance” [23, 26–29], “Cluster” [32–35], “Dual” [24, 25, 36], and “Others” [30, 44, 59–64] methods.

1) Comparison on VeRi776: From Table I, it can be found that the proposed TCRL method achieves the highest mAP (i.e., 42.68%), rank1 (i.e., 87.26%), and rank5 (i.e., 90.75%),

TABLE III

THE TCRL ABLATION EXPERIMENTS ON VERI776. “DIRECTLY” DENOTES DIRECTLY MODELS THE PART FEATURES AND GLOBAL FEATURES.

Setting	mAP	Rank1	Rank5	Rank10
Directly	2.19	12.61	19.84	26.37
Clustering in Part Branch	31.74	70.28	78.41	82.66
w/o Part Branch	41.72	85.17	87.26	88.93
w/ Stop-gradient	42.47	86.76	89.61	90.85
TCRL	<b>42.68</b>	<b>87.26</b>	<b>90.75</b>	<b>91.68</b>

which respectively outperforms the CACL [25] (2nd place) by 2.76%, 2.80%, and 2.54%, due to considering part features, introducing all negative instances, and fixing mislabeled images. We have also observed the “Cluster”, “Dual”, and “Others” methods are mostly superior to the “Instance” methods on the VeRi776 dataset by a large margin, indicating the importance of same-category correlations for unsupervised learning. Then, compared to the “Cluster” methods, the mAP and rank1 of the proposed TCRL approach exceeds 2.18% and 2.06 % over the best “Cluster” method (i.e.,UCF [35]). It is noteworthy that UCF method uses an additional vehicle dataset (i.e., VehicleID), whereas our proposed TCRL does not require any additional training set. Moreover, on mAP, rank1, and rank5, the proposed TCRL method is even significantly better than the ML [64] method using semantic information, which proves the direct introduction of part features can better learn fine-grained semantic information.

2) Comparison on VehicleID: In fact, the VehicleID [66] dataset has a larger data scale than the VeRi776 [65] dataset. However, the proposed TCRL method still can obtain the 1st place and outperforms those state-of-the-art methods under comparison, as occurred on the VeRi776 dataset, as shown in Table II. For example, on Test800, Test1600, and Test2400, the proposed TCRL method respectively higher than the best “Cluster” method, i.e., CCL [34], 3.65%, 3.67%, and 3.60% on rank1. Moreover, we compare our proposed TCRL with the most competing method CACL [25], which employs both instance memory bank and cluster memory bank for

TABLE IV  
EVALUATION THE ROLE (%) OF THE DIFFERENT LOSS FUNCTION ON THE VERI776 AND VEHICLEID DATASETS.

Setting	VeRi776		VehicleID					
	mAP	Rank1	Test800		Test1600		Test2400	
			mAP	Rank1	mAP	Rank1	mAP	Rank1
Baseline ( $L_{CCL}$ )	40.30	84.60	62.97	56.71	60.10	52.55	57.08	49.33
$L_{WRCCL}$	41.18	85.52	64.74	58.68	62.29	54.07	59.22	51.55
$L_{HCL}$	41.33	85.79	65.01	58.93	62.67	54.42	59.74	51.96
$L_{PCL}$	41.58	85.90	65.26	59.18	62.84	54.61	59.79	52.07
$L_{ID} + L_{Triplet}$	38.82	83.05	59.27	53.65	55.18	48.36	53.40	45.67
$L_{ID} + L_{CCL}$	40.38	84.71	63.12	56.84	60.25	52.72	57.23	49.41
$L_{WRCCL} + L_{HCL}$	41.83	86.64	65.38	59.41	62.96	54.88	59.90	52.31
$L_{WRCCL} + L_{PCL}$	41.86	86.59	65.51	59.67	63.22	55.06	60.23	52.44
$L_{HCL} + L_{PCL}$	42.15	86.47	65.75	59.92	63.28	55.27	60.31	52.47
$L_{CCL} + L_{ID} + L_{Triplet}$	40.61	85.07	63.33	57.18	60.49	52.96	57.46	49.68
TCRL ( $L_{CCL} + L_{ID} + L_{Triplet}$ )	41.34	86.02	64.74	58.65	61.88	54.11	59.23	51.36
<b>TCRL (<math>L_{WRCCL} + L_{HCL} + L_{PCL}</math>)</b>	<b>42.68</b>	<b>87.26</b>	<b>66.29</b>	<b>60.36</b>	<b>63.74</b>	<b>56.22</b>	<b>61.08</b>	<b>52.93</b>

contrastive loss, but CACL underestimates part features and ignores all negative samples. Based on the differences above, our TCRL method leads to 2.46% improvements in mAP and up to 2.59% gains in rank1 on Test800.

3) *Comparison on VERI-Wild*: The VERI-Wild [68] is a much larger dataset than VeRi776 [65] and VehicleID [66], Table II shows that the proposed TCRL method wins the 1st place among all compared state-of-the-art methods. First, the “Instance” methods (i.e., MoCo [26] and SimSiam [29]) can not acquire promising accuracies, which are inferior to the proposed TCRL method and other three categories approaches. Second, the proposed TCRL method has better performance than those “Cluster” methods. For example, taking the “Cluster” methods with the cluster memory bank, i.e., CACL [25], it is still defeated by the proposed TCRL method, as it has lower mAP and rank1 on three different testing subsets (i.e., Test3000, Test5000 and Test1000). Third, on largest Test1000 subset, mAP and rank1 of TCRL method respectively are 4.00% and 8.41% higher than those of the best “Others” method, i.e., VAPC [45], which extra uses an viewpoint-aware module. Meanwhile, the proposed TCRL method obtains the state-of-the-art performance on VeRi776, VehicleID, and VERI-Wild, which shows the effectiveness and robustness of our method.

#### D. Ablation Studies

In this section, we analyze the proposed TCRL from seven aspects: (1) Advantage of TCRL design, (2) Impact of each loss function, (3) Influence of mask sampling strategy, (4) Impact of momentum value, (5) Impact of batch size, (6) Role of different updating polices for cluster memory bank, and (7) Qualitative Samples.

1) *Advantage of TCRL Design*: To validate the effectiveness and superiority of TCRL, we pay special attention to designs that may affect model performance, whose result is shown in Table Table III. The model does not work if it directly models the part features and global features. Collapsing is observed (first row of Table III) due to  $M^P$  and  $M^G$  are identity mapping. Then we tried to generate pseudo-labels

using part features, but the performance (31.74% vs. 42.68% mAP) dropped significantly, indicating clustering based on part features is very difficult and not applicable. We have also observed that a sufficient part feature is crucial role in vehicle re-identification. For example, TCRL respectively defeats w/o part branch 2.09% and 3.46% accuracy on Rank1 and Rank5.

Besides, we also find an interesting phenomenon, using stop-gradient is not necessary for TCRL design. As shown in Table III, w/ stop-gradient is comprehensively higher than clustering in part branch and w/o part branch in terms of mAP, Rank1, Rank5, and Rank10 accuracy, but only slightly lower than TCRL. Because we use a proxy strategy (i.e., cluster feature  $c_k$ ) instead of directly performing contrastive learning with global and part features. Overall, it is reasonable and efficient for default TCRL to give a solution on how to utilize part features in supervised re-identification.

2) *Impact of Loss Functions*: We conduct a set of experiments by disabling each loss function in our proposed TCRL individually, i.e., hybrid contrastive loss  $L_{HCL}$ , weighted regularization cluster contrastive loss  $L_{WRCCL}$ , and proxy contrastive loss  $L_{PCL}$ . Noted that the ‘Baseline’ denotes the result of using only cluster contrastive loss (CCL) [34]. The ablation experimental results are shown in Table IV.

From Table IV, all setting methods have all consistently outperformed Baseline method on two datasets. Especially  $L_{WRCCL}$  is better than Baseline by more than 2.22 % Rank1 on the largest Test2400, which demonstrates that  $L_{WRCCL}$  can well penalize mislabeled images to improve performance. Then, we can find that using both proposed loss functions simultaneously gives better results than using one loss function alone, which shows that different loss functions can be mutually compatible and mutually reinforcing. Furthermore, we find that the network using  $L_{WRCCL}$ ,  $L_{HCL}$ , and  $L_{PCL}$  instead of triplet loss or ID loss could also reach a competitive performance. For example,  $L_{HCL} + L_{PCL}$  respectively improves the performance of the  $L_{ID} + L_{Triplet}$  and  $L_{ID} + L_{CCL}$  by 6.91% and 3.08% mAP on the largest Test2400.

Besides, we show the performance drops when one loss function is disabled individually, as shown in Table IV. For example, TCRL respectively defeats the  $L_{WRCCL} + L_{HCL}$ ,

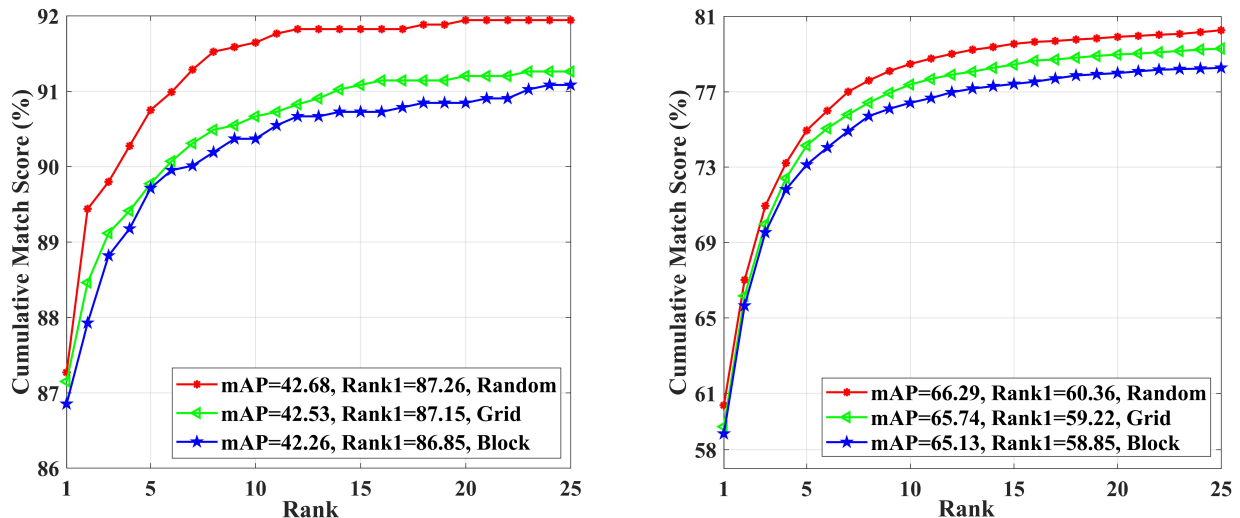


Fig. 4. The CMC curves on VeRi776 and VehicleID. Different methods are compared from Rank1 to Rank25.

TABLE V  
DIFFERENT UPDATE POLICIES FOR THE CLUSTER MEMORY BANK.

Setting	VeRi776		VehicleID					
	mAP	Rank1	Test800		Test1600		Test2400	
	mAP	Rank1	mAP	Rank1	mAP	Rank1	mAP	Rank1
Random	40.89	85.17	63.45	57.83	61.70	54.03	58.96	50.51
Hard	42.06	86.76	65.82	59.77	63.06	55.85	60.36	51.93
All	<b>42.68</b>	<b>87.26</b>	<b>66.29</b>	<b>60.36</b>	<b>63.74</b>	<b>56.22</b>	<b>61.08</b>	<b>52.93</b>

$L_{WRCCl} + L_{PCL}$ , and  $L_{HCL} + L_{PCL}$  by 0.85 %, 0.82% and 0.53 % in term of mAP on VeRi776. These results show that each loss contributes to the performance improvements. More importantly, compared to Baseline ( $L_{CCL}$ ) and  $L_{CCL} + L_{ID} + L_{Triplet}$ ,  $TCRL(L_{WRCCl} + L_{HCL} + L_{PCL})$  achieves a total gain of 3.32% and 2.96% on mAP accuracy of Test800. Because TCRL simultaneously constrains global, part, and cluster features, CCL does not have a part branch and only constrains the global features. This choice is natural since part features can boost performance further in supervised re-identification.

3) **Influence of Mask Sampling:** We compare three common mask sampling strategies, results as shown in Fig. 4. The Random denotes the default strategy used in this paper, see Section IV-B for details. The Grid represents that the default setting is used for grid mask, and the details of its can be found in [70]. The Block means to randomly delete an area whose area is 30% of the original image. The 30% is empirical results obtained through cross-validation.

Fig. 4 reveals an intuitive situation that from rank1 to rank25, the performance of Grid has consistently outperformed Block, which shows that the mask of the whole area (30% entire image) is detrimental to learning discriminative features of vehicles. Then, the Random method is significantly better than Grid and Block in the performance of rank1 and mAP on VeRi776 and VehicleID. For example, Random method are 1.14% and 1.51% mAP higher than Grid and Block on Test800 of VehicleID. Because Grid uses regular structured masks

on all images, which easily leads the network to overfit this regular mask when learning part features. In contrast, Random has a random irregular sampling with a high mask rate, which makes the network need to learn good representations for all the patches, and to mine discriminative part features from the patches. These results demonstrate that simple random mask works best for our proposed TCRL method, resulting in good performance on two datasets.

4) **Impact of Momentum Value:** As shown in Fig. 5, we adopt a momentum update strategy to refresh the part memory bank  $M^P$ , global memory bank  $M^G$ , and cluster memory bank  $M^C$ . And the momentum value  $\alpha$ ,  $\beta$ , and  $\gamma$  controls the update speed of the memory banks. The three memory banks use the same momentum value, that is,  $\alpha = \beta = \gamma$  in the Eq. 8 and Eq. 11. From Fig. 5, when the momentum value is 0.1, the mAP performance is the highest on the VeRi776 and VehicleID datasets. When the momentum value is greater than 0.5, the results of mAP drop significantly. Therefore, we set  $\alpha = \beta = \gamma = 0.1$  in this paper.

5) **Impact of Batch Size:** We evaluate the performance impact of different batch sizes on proposed TCRL method. The Fig. 5, shows the mAP performance for batch sizes from 64 to 192 on VeRi776 and VehicleID. Overall, the performance of our method can remain stable in the batch size range of 64 to 192. Compared with the state-of-the-art methods in Table I and Table II, our method achieves superior performance on regular batch sizes. Especially, using a batch size of 128 can respectively get the highest 42.68% and 66.29% on two

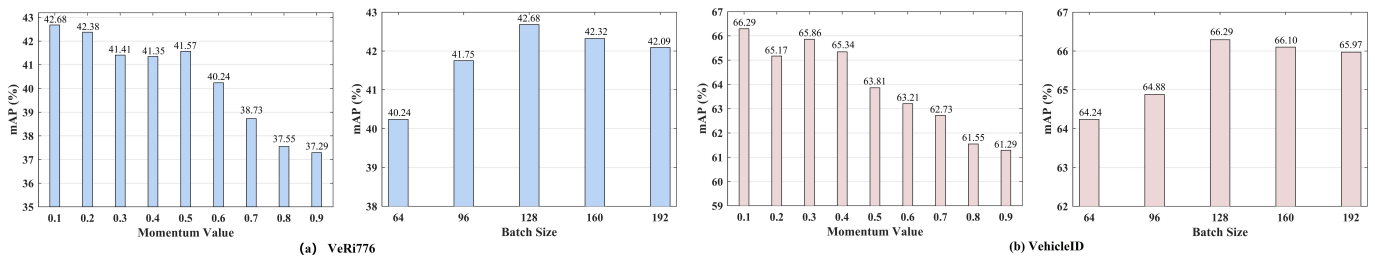


Fig. 5. The impact of momentum value and batch size on VeRi776 and VehicleID. Different parameters are compared on mAP.



Fig. 6. Qualitative examples of cases. The first and second rows show the top five images returned by Baseline and TCRL, respectively. Images with blue, green, and red boxes denote query ID, correct, and incorrect retrieve results.

datasets, which is higher than the batch size of 64 and 192. Thus we choose 128 as our default batch size setting.

6) **Role of Different Updating Polices for Cluster Memory Bank:** There are three update strategies for cluster memory bank  $M_C$ , namely random update strategy, hard update strategy, and all update strategy. The “Random” and “Hard” denote that we update the cluster memory bank  $M_C$  with one random sample per class and the least similar sample in each class, respectively. The “All” indicates that all sample is used to update the cluster memory bank  $M_C$ . The corresponding results are shown in Table V. The “ALL” strategies achieve the highest 42.68% mAP and 87.26% rank1 on VeRi776. Therefore, like most existing works [34], we choose the ‘All’ update strategy for cluster memory bank  $M_C$  in this work.

7) **Qualitative Samples:** To demonstrate some qualitative results of our proposed TCRL, we present rank list visualization in Fig. 6. Images with blue, green, and red boxes denote query ID, correct, and incorrect retrieve results, respectively. The Rank1-5 errors of Baseline are often caused by vehicles with highly similar backgrounds and viewpoints, while the TCRL performed well and had more correct images in the rank list. Because we specially designed the  $M^p$  and three different loss functions to focus on part features and penalize negative samples. These results demonstrate that the proposed TCRL can effectively capture the specific hints for each part.

## V. CONCLUSIONS

This paper presents a simple Triplet Contrastive Representation Learning (TCRL) framework, which leverages cluster features to bridge the part and global features. Specifically, TCRL devises three memory banks to store the features according to their attributes. Then a Proxy Contrastive Loss (PCL)

is proposed to make contrastive learning between adjacent memory banks, thus presenting the associations between the part and global features as the part-cluster and the cluster-global associations. To achieve higher performance, TCRL proposes two additional loss functions, the Hybrid Contrastive Loss (HCL) to re-define the sample correlations by approaching the positive cluster features and leaving all the negative instance features, and the Weighted Regularization Cluster Contrastive Loss (WRCCCL) to refine the pseudo labels via penalizing the mislabeled images. Extensive experimental results on three vehicle re-ID datasets, VeRi776, VehicleID, and VERI-Wild demonstrate that our method can be superior to state-of-the-art methods. In the future, we hope our exploration will motivate people to rethink the roles of part features for unsupervised vehicle re-identification.

## REFERENCES

- [1] D. Shen, S. Zhao, J. Hu, H. Feng, D. Cai, and X. He, “Es-net: Erasing salient parts to learn more in re-identification,” *IEEE Transactions on Image Processing*, vol. 30, pp. 1676–1686, 2020.
- [2] X. Liu, S. Zhang, X. Wang, R. Hong, and Q. Tian, “Group-group loss-based global-regional feature learning for vehicle re-identification,” *IEEE Transactions on Image Processing*, vol. 29, pp. 2638–2652, 2019.
- [3] H. Li, C. Li, A. Zheng, J. Tang, and B. Luo, “Attribute and state guided structural embedding network for vehicle re-identification,” *IEEE transactions on image processing*, vol. 31, pp. 5949–5962, 2022.
- [4] W. Wang, F. Zhao, S. Liao, and L. Shao, “Attentive waveblock: Complementarity-enhanced mutual networks for unsupervised domain adaptation in person re-identification and beyond,” *IEEE Transactions on Image Processing*, vol. 31, pp. 1532–1544, 2022.
- [5] H. Guo, K. Zhu, M. Tang, and J. Wang, “Two-level attention network with multi-grain ranking loss for vehicle re-identification,” *IEEE Transactions on Image Processing*, vol. 28, no. 9, pp. 4328–4338, 2019.
- [6] H. Luo, W. Jiang, Y. Gu, F. Liu, X. Liao, S. Lai, and J. Gu, “A strong baseline and batch normalization neck for deep person re-identification,” *IEEE Transactions on Multimedia*, vol. 22, no. 10, pp. 2597–2609, 2019.
- [7] X. Liu, W. Liu, J. Zheng, C. Yan, and T. Mei, “Beyond the parts: Learning multi-view cross-part correlation for vehicle re-identification,” in *Proceedings of the 28th*

- ACM International Conference on Multimedia*, 2020, pp. 907–915.
- [8] R. Chu, Y. Sun, Y. Li, Z. Liu, C. Zhang, and Y. Wei, “Vehicle re-identification with viewpoint-aware metric learning,” in *International Conference on Computer Vision*, 2019, pp. 8282–8291.
- [9] S. He, H. Luo, P. Wang, F. Wang, H. Li, and W. Jiang, “Transreid: Transformer-based object re-identification,” in *Proceedings of the IEEE/CVF International Conference on Computer Vision*, 2021, pp. 15 013–15 022.
- [10] F. Shen, J. Zhu, X. Zhu, J. Huang, H. Zeng, Z. Lei, and C. Cai, “An efficient multi-resolution network for vehicle re-identification,” *IEEE Internet of Things Journal*, 2021.
- [11] P. Wang, C. Ding, W. Tan, M. Gong, K. Jia, and D. Tao, “Uncertainty-aware clustering for unsupervised domain adaptive object re-identification,” *IEEE Transactions on Multimedia*, 2022.
- [12] Q. Wang, W. Min, Q. Han, Q. Liu, C. Zha, H. Zhao, and Z. Wei, “Inter-domain adaptation label for data augmentation in vehicle re-identification,” *IEEE Transactions on Multimedia*, vol. 24, pp. 1031–1041, 2021.
- [13] M. Li, J. Liu, C. Zheng, X. Huang, and Z. Zhang, “Exploiting multi-view part-wise correlation via an efficient transformer for vehicle re-identification,” *IEEE Transactions on Multimedia*, 2021.
- [14] Z. Zheng, T. Ruan, Y. Wei, Y. Yang, and T. Mei, “Vehiclenet: Learning robust visual representation for vehicle re-identification,” *IEEE Transactions on Multimedia*, vol. 23, pp. 2683–2693, 2020.
- [15] X. Lin, R. Li, X. Zheng, P. Peng, Y. Wu, F. Huang, and R. Ji, “Aggregating global and local visual representation for vehicle re-identification,” *IEEE Transactions on Multimedia*, vol. 23, pp. 3968–3977, 2020.
- [16] T. Si, F. He, Z. Zhang, and Y. Duan, “Hybrid contrastive learning for unsupervised person re-identification,” *IEEE Transactions on Multimedia*, 2022.
- [17] M. Ye, J. Shen, G. Lin, T. Xiang, L. Shao, and S. C. Hoi, “Deep learning for person re-identification: A survey and outlook,” *IEEE Transactions on Pattern Analysis and Machine Intelligence*, 2021.
- [18] M. Ye, A. J. Ma, L. Zheng, J. Li, and P. C. Yuen, “Dynamic label graph matching for unsupervised video re-identification,” in *International Conference on Computer Vision*, 2017, pp. 5142–5150.
- [19] M. Ye, J. Li, A. J. Ma, L. Zheng, and P. C. Yuen, “Dynamic graph co-matching for unsupervised video-based person re-identification,” *IEEE Transactions on Image Processing*, vol. 28, no. 6, pp. 2976–2990, 2019.
- [20] M. Ye, X. Lan, and P. C. Yuen, “Robust anchor embedding for unsupervised video person re-identification in the wild,” in *Proceedings of the European Conference on Computer Vision (ECCV)*, 2018, pp. 170–186.
- [21] R. Wei, J. Gu, S. He, and W. Jiang, “Transformer-based domain-specific representation for unsupervised domain adaptive vehicle re-identification,” *IEEE Transactions on Intelligent Transportation Systems*, 2022.
- [22] H. Luo, P. Wang, Y. Xu, F. Ding, Y. Zhou, F. Wang, H. Li, and R. Jin, “Self-supervised pre-training for transformer-based person re-identification,” *arXiv preprint arXiv:2111.12084*, 2021.
- [23] T. Chen, S. Kornblith, M. Norouzi, and G. Hinton, “A simple framework for contrastive learning of visual representations,” in *International conference on machine learning*. PMLR, 2020, pp. 1597–1607.
- [24] Z. Hu, C. Zhu, and G. He, “Hard-sample guided hybrid contrast learning for unsupervised person re-identification,” in *2021 7th IEEE International Conference on Network Intelligence and Digital Content (IC-NIDC)*. IEEE, 2021, pp. 91–95.
- [25] M. Li, C.-G. Li, and J. Guo, “Cluster-guided asymmetric contrastive learning for unsupervised person re-identification,” *IEEE Transactions on Image Processing*, vol. 31, pp. 3606–3617, 2022.
- [26] K. He, H. Fan, Y. Wu, S. Xie, and R. Girshick, “Momentum contrast for unsupervised visual representation learning,” in *Proceedings of the IEEE/CVF conference on computer vision and pattern recognition*, 2020, pp. 9729–9738.
- [27] M. Caron, I. Misra, J. Mairal, P. Goyal, P. Bojanowski, and A. Joulin, “Unsupervised learning of visual features by contrasting cluster assignments,” *Advances in Neural Information Processing Systems*, vol. 33, pp. 9912–9924, 2020.
- [28] J.-B. Grill, F. Strub, F. Altché, C. Tallec, P. Richemond, E. Buchatskaya, C. Doersch, B. Avila Pires, Z. Guo, M. Gheshlaghi Azar *et al.*, “Bootstrap your own latent—a new approach to self-supervised learning,” *Advances in Neural Information Processing Systems*, vol. 33, pp. 21 271–21 284, 2020.
- [29] X. Chen and K. He, “Exploring simple siamese representation learning,” in *Proceedings of the IEEE/CVF Conference on Computer Vision and Pattern Recognition*, 2021, pp. 15 750–15 758.
- [30] Y. Lin, X. Dong, L. Zheng, Y. Yan, and Y. Yang, “A bottom-up clustering approach to unsupervised person re-identification,” in *Proceedings of the AAAI Conference on Artificial Intelligence*, vol. 33, no. 01, 2019, pp. 8738–8745.
- [31] M. Ye, X. Zhang, P. C. Yuen, and S.-F. Chang, “Unsupervised embedding learning via invariant and spreading instance feature,” in *Proceedings of the IEEE/CVF Conference on Computer Vision and Pattern Recognition*, 2019, pp. 6210–6219.
- [32] Y. Ge, F. Zhu, D. Chen, R. Zhao *et al.*, “Self-paced contrastive learning with hybrid memory for domain adaptive object re-id,” *Advances in Neural Information Processing Systems*, vol. 33, pp. 11 309–11 321, 2020.
- [33] X. Li, T. Liang, Y. Jin, T. Wang, and Y. Li, “Camera-aware style separation and contrastive learning for unsupervised person re-identification,” *arXiv preprint arXiv:2112.10089*, 2021.
- [34] Z. Dai, G. Wang, W. Yuan, S. Zhu, and P. Tan, “Cluster contrast for unsupervised person re-identification,” in *Proceedings of the Asian Conference on Computer Vision*, 2022, pp. 1142–1160.
- [35] P. Wang, C. Ding, W. Tan, M. Gong, K. Jia, and D. Tao,

- “Uncertainty-aware clustering for unsupervised domain adaptive object re-identification,” *IEEE Transactions on Multimedia*, 2022.
- [36] H. Sun, M. Li, and C.-G. Li, “Hybrid contrastive learning with cluster ensemble for unsupervised person re-identification,” *arXiv preprint arXiv:2201.11995*, 2022.
- [37] Y. Sun, L. Zheng, Y. Yang, Q. Tian, and S. Wang, “Beyond part models: Person retrieval with refined part pooling (and a strong convolutional baseline),” in *European Conference on Computer Vision*, 2018, pp. 480–496.
- [38] P. Khorramshahi, A. Kumar, N. Peri, S. S. Rambhatla, J.-C. Chen, and R. Chellappa, “A dual-path model with adaptive attention for vehicle re-identification,” in *International Conference on Computer Vision*, 2019, pp. 6132–6141.
- [39] Y. Lou, Y. Bai, J. Liu, S. Wang, and L.-Y. Duan, “Embedding adversarial learning for vehicle re-identification,” *IEEE Transactions on Image Processing*, vol. 28, no. 8, pp. 3794–3807, 2019.
- [40] Y. Zhou, L. Liu, and L. Shao, “Vehicle re-identification by deep hidden multi-view inference,” *IEEE Transactions on Image Processing*, vol. 27, no. 7, pp. 3275–3287, 2018.
- [41] F. Shen, Y. Xie, J. Zhu, X. Zhu, and H. Zeng, “Git: Graph interactive transformer for vehicle re-identification,” *IEEE Transactions on Image Processing*, 2023.
- [42] F. Shen, X. Peng, L. Wang, X. Hao, M. Shu, and Y. Wang, “Hsgm: A hierarchical similarity graph module for object re-identification,” in *2022 IEEE International Conference on Multimedia and Expo (ICME)*. IEEE, 2022, pp. 1–6.
- [43] J. Zbontar, L. Jing, I. Misra, Y. LeCun, and S. Deny, “Barlow twins: Self-supervised learning via redundancy reduction,” in *International Conference on Machine Learning*. PMLR, 2021, pp. 12 310–12 320.
- [44] J. Peng, H. Wang, F. Xu, and X. Fu, “Cross domain knowledge learning with dual-branch adversarial network for vehicle re-identification,” *Neurocomputing*, vol. 401, pp. 133–144, 2020.
- [45] A. Zheng, X. Sun, C. Li, and J. Tang, “Aware progressive clustering for unsupervised vehicle re-identification,” *IEEE Transactions on Intelligent Transportation Systems*, 2021.
- [46] H. Chen, B. Lagadec, and F. Bremond, “Partition and reunion: A two-branch neural network for vehicle re-identification,” in *Conference on Computer Vision and Pattern Recognition Workshops*, 2019, pp. 184–192.
- [47] F. Shen, J. Zhu, X. Zhu, Y. Xie, and J. Huang, “Exploring spatial significance via hybrid pyramidal graph network for vehicle re-identification,” *IEEE Transactions on Intelligent Transportation Systems*, 2021.
- [48] J. Qian, W. Jiang, H. Luo, and H. Yu, “Stripe-based and attribute-aware network: A two-branch deep model for vehicle re-identification,” *Measurement Science and Technology*, vol. 31, no. 9, p. 095401, 2020.
- [49] H. Guo, K. Zhu, M. Tang, and J. Wang, “Two-level attention network with multi-grain ranking loss for vehicle re-identification,” *IEEE Transactions on Image Processing*, pp. 4328–4338, 2019.
- [50] C. Liu, D. Q. Huynh, and M. Reynolds, “Urban area vehicle re-identification with self-attention stair feature fusion and temporal bayesian re-ranking,” in *International Joint Conference on Neural Networks*, 2019, pp. 1–8.
- [51] M. Li, M. Wei, X. He, and F. Shen, “Enhancing part features via contrastive attention module for vehicle re-identification,” in *2022 IEEE International Conference on Image Processing (ICIP)*. IEEE, 2022, pp. 1816–1820.
- [52] B. He, J. Li, Y. Zhao, and Y. Tian, “Part-regularized near-duplicate vehicle re-identification,” in *Conference on Computer Vision and Pattern Recognition*, 2019, pp. 3997–4005.
- [53] X. Zhang, R. Zhang, J. Cao, D. Gong, M. You, and C. Shen, “Part-guided attention learning for vehicle re-identification,” *arXiv preprint arXiv:1909.06023*, 2019.
- [54] Y. Sun, M. Li, and J. Lu, “Part-based multi-stream model for vehicle searching,” in *International Conference on Pattern Recognition*, 2018, pp. 1372–1377.
- [55] J. Redmon, S. Divvala, R. Girshick, and A. Farhadi, “You only look once: Unified, real-time object detection,” in *Conference on Computer Vision and Pattern Recognition*, 2016, pp. 779–788.
- [56] K. He, X. Zhang, S. Ren, and J. Sun, “Deep residual learning for image recognition,” in *Conference on Computer Vision and Pattern Recognition*, 2016, pp. 770–778.
- [57] M. Ester, H.-P. Kriegel, J. Sander, X. Xu *et al.*, “A density-based algorithm for discovering clusters in large spatial databases with noise.” in *kdd*, vol. 96, no. 34, 1996, pp. 226–231.
- [58] G. Hinton, O. Vinyals, J. Dean *et al.*, “Distilling the knowledge in a neural network,” *arXiv preprint arXiv:1503.02531*, vol. 2, no. 7, 2015.
- [59] T. Xiao, S. Li, B. Wang, L. Lin, and X. Wang, “Joint detection and identification feature learning for person search,” in *Proceedings of the IEEE conference on computer vision and pattern recognition*, 2017, pp. 3415–3424.
- [60] H. Fan, L. Zheng, C. Yan, and Y. Yang, “Unsupervised person re-identification: Clustering and fine-tuning,” *ACM Transactions on Multimedia Computing, Communications, and Applications (TOMM)*, vol. 14, no. 4, pp. 1–18, 2018.
- [61] Z. Zhong, L. Zheng, S. Li, and Y. Yang, “Generalizing a person retrieval model hetero-and homogeneously,” in *Proceedings of the European conference on computer vision (ECCV)*, 2018, pp. 172–188.
- [62] Z. Zhong, L. Zheng, Z. Luo, S. Li, and Y. Yang, “Invariance matters: Exemplar memory for domain adaptive person re-identification,” in *Proceedings of the IEEE/CVF Conference on Computer Vision and Pattern Recognition*, 2019, pp. 598–607.
- [63] L. Song, C. Wang, L. Zhang, B. Du, Q. Zhang, C. Huang, and X. Wang, “Unsupervised domain adaptive re-identification: Theory and practice,” *Pattern Recognition*, vol. 102, p. 107173, 2020.

- [64] H. Wang, J. Peng, G. Jiang, and X. Fu, “Learning multiple semantic knowledge for cross-domain unsupervised vehicle re-identification,” in *2021 IEEE International Conference on Multimedia and Expo (ICME)*. IEEE, 2021, pp. 1–6.
- [65] X. Liu, W. Liu, T. Mei, and H. Ma, “A deep learning-based approach to progressive vehicle re-identification for urban surveillance,” in *European Conference on Computer Vision*, 2016, pp. 869–884.
- [66] H. Liu, Y. Tian, Y. Wang, L. Pang, and T. Huang, “Deep relative distance learning: Tell the difference between similar vehicles,” in *Conference on Computer Vision and Pattern Recognition*, 2016, pp. 2167–2175.
- [67] Q. Xiao, K. Cao, H. Chen, F. Peng, and C. Zhang, “Cross domain knowledge transfer for person re-identification,” *arXiv preprint arXiv:1611.06026*, 2016.
- [68] Y. Lou, Y. Bai, J. Liu, S. Wang, and L. Duan, “Veri-wild: A large dataset and a new method for vehicle re-identification in the wild,” in *Conference on Computer Vision and Pattern Recognition*, 2019, pp. 3235–3243.
- [69] A. Paszke, S. Gross, F. Massa, A. Lerer, J. Bradbury, G. Chanan, T. Killeen, Z. Lin, N. Gimeshain, L. Antiga, A. Desmaison, A. Kopf, E. Yang, Z. DeVito, M. Raison, A. Tejani, S. Chilamkurthy, B. Steiner, L. Fang, J. Bai, and S. Chintala, “Pytorch: An imperative style, high-performance deep learning library,” in *Advances in Neural Information Processing Systems*, 2019, pp. 8024–8035.
- [70] P. Chen, S. Liu, H. Zhao, and J. Jia, “Gridmask data augmentation,” *arXiv preprint arXiv:2001.04086*, 2020.